The effect of oriented microcracks and crystallographic and shape preferred orientation on bulk elastic anisotropy of a foliated biotite gneiss from Outokumpu

ARTICLE *in* TECTONOPHYSICS · OCTOBER 2008

Impact Factor: 2.87 · DOI: 10.1016/j.tecto.2008.06.015

5 AUTHORS, INCLUDING:

Tatiana I. Ivankina
Joint Institute for Nuclear Research
34 PUBLICATIONS **154** CITATIONS

Tectonophysics 457 (2008) 143–149

Contents lists available at ScienceDirect

Tectonophysics

journal homepage: www.elsevier.com/locate/tecto

The effect of oriented microcracks and crystallographic and shape preferred orientation on bulk elastic anisotropy of a foliated biotite gneiss from Outokumpu

H. Kern [a,*], T.I. Ivankina [b], A.N. Nikitin [b], T. Lokajíček [c], Z. Pros [c]

[a] Institute für Geowissenschaften, Universität Kiel, Olshausenstr. 40, D-24098 Kiel, Germany
[b] Joint Institute for Nuclear Research, Frank Laboratory of Neutron Physics, 141980 Dubna, Moscow Region, Russia
[c] Institute of Geology, Academy of Sciences of the Czech Republic, Rozvojová 269, 165 00 Prague 6, Czech Republic

ARTICLE INFO

Article history:
Received 27 March 2008
Received in revised form 3 June 2008
Accepted 3 June 2008
Available online 19 June 2008

Keywords:
Biotite gneiss
Velocity measurements
Seismic anisotropy
Microcracks
Lattice preferred orientation
Shape preferred orientation

ABSTRACT

Elastic anisotropy is an important property of crustal and mantle rocks. This study investigates the contribution of oriented microcracks and crystallographic (LPO) and shape preferred orientation (SPO) to the bulk elastic anisotropy of a strongly foliated biotite gneiss, using different methodologies. The rock is felsic in composition (about 70 vol.% SiO_2) and made up by about 40 vol.% quartz, 37 vol.% plagioclase and 23 vol.% biotite. Measurements of compressional (Vp) and shear wave (Vs) velocities on a sample cube in the three foliation-related structural directions (up to 600 MPa) and of the 3D P-wave velocity distribution on a sample sphere (up to 200 MPa) revealed a strong pressure sensitivity of Vp, Vs and P-wave anisotropy in the low pressure range. A major contribution to bulk anisotropy is from biotite. Importantly, intercrystalline and intracrystalline cracks are closely linked to the morphologic sheet plane (001) of the biotite minerals, leading to very high anisotropy at low pressure. Above about 150 MPa the effect of cracks is almost eliminated, due to progressive closure of microcracks. The residual (pressure-independent) part of velocity anisotropy is mainly caused by the strong alignment of the platy biotite minerals, displaying a strong SPO and LPO. Calculation of the 3D velocity distribution based on neutron diffraction texture measurements of biotite, quartz, and plagioclase and their single-crystal properties give evidence for an important contribution of the biotite LPO to the intrinsic velocity anisotropy, confirming the experimental findings that maximum and minimum velocities and shear wave splitting are closely related to foliation. Comparison of the LPO-based calculated anisotropy (about 8%) with measured intrinsic anisotropy (about 15% at 600 MPa) give hints for a major contribution of SPO to the bulk anisotropy of the rock.

1. Introduction

Most of the rocks constituting the Earth's crust (e.g., gneisses, amphibolites, granulites) and the upper mantle (peridotites, dunites) exhibit marked anisotropy of elastic properties (e.g. Christensen, 1984; Burlini and Fountain, 1993; Barruol and Kern, 1996; Kern et al., 2001). Anisotropy may be caused (1) by lattice (or crystallographic) preferred orientation (LPO), (2) by preferred morphological (or shape) preferred orientation (SPO), (3) by preferred orientation of microcracks, and (4) by thin layers of otherwise isotropic materials with different properties.

In this study we investigate to which extent oriented microcracks, LPO and SPO of the constituent minerals contribute to the bulk elastic anisotropy of a strongly foliated gneiss recovered from the Outokumpu Scientific Deep Drill Hole. This rock type constitutes about 70 vol.% of the 2500 m thick crustal section penetrated by the borehole. Experimental and theoretical approaches are used to investigate the nature of seismic anisotropy in the rock. We will first measure P- and S-wave velocities in different directions as a function of pressure and then compare the experimental data with those obtained from 3D velocity calculations based on neutron diffraction texture measurements.

2. Sample description and methods

The samples used for the investigations were prepared from a drill core (10 cm in diameter and about 10 cm in length) retrieved from 818 m depth. For the laboratory seismic measurements a sample cube (43 mm on edges) as well as a sample sphere (30 mm in diameter) were taken from the center of the core, ensuring that disturbance of the microstructure by drilling was minimized.

The biotite gneiss is felsic in composition (70.16 wt.% SiO_2) and made up by 39.9 vol.% quartz, 37.4 vol.% plagioclase, 22.6 vol.% biotite and iron sulfide (0.1 vol.%) as an accessory mineral. It is fine-grained and exhibits strong shape preferred orientation (SPO) of the platy mica grains, which define the foliation. The grain sizes vary between 0.05 and 2 mm (length) and 5 μm and 200 μm (width). Fig. 1 presents microstructures from thin sections cut along the *ZY*- and *ZX*-plane, according to the structural frame (*XY* is foliation, *X* is lineation and *Z* is foliation normal). Fig. 1b shows that the orientation of the platy biotite

* Corresponding author.
E-mail address: kern@min.uni-kiel.de (H. Kern).

0040-1951/$ – see front matter © 2008 Elsevier B.V. All rights reserved.
doi:10.1016/j.tecto.2008.06.015

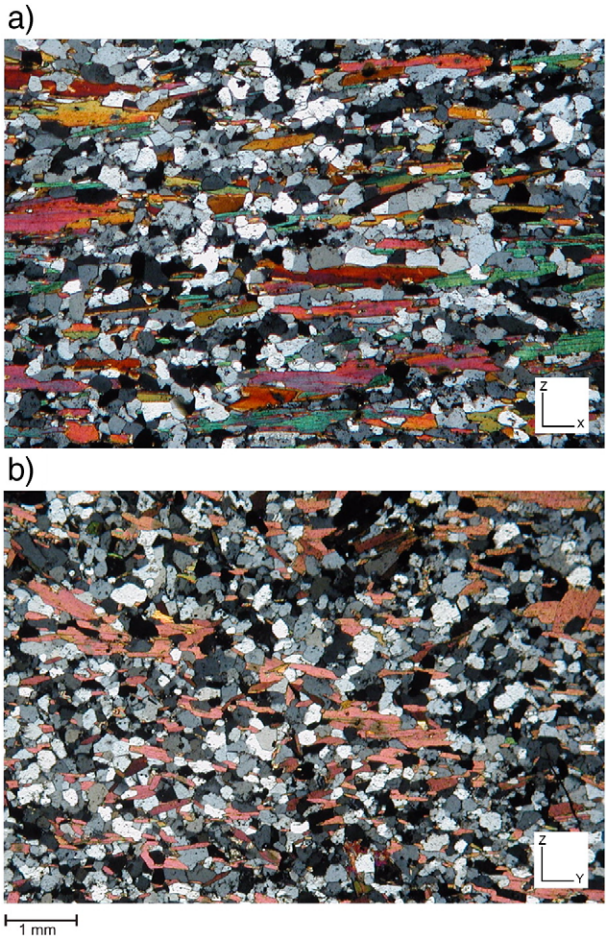

Fig. 1. Optical microphotographs showing microstructures of biotite gneiss sample 818. (a) Section cut normal to foliation and parallel to lineation (*ZX* plane). (b) Section cut normal to foliation and normal to lineation (*ZY* plane). Foliation is defined by a strong shape preferred orientation (SPO) of the platy biotite minerals.

minerals fluctuates around the *X* direction giving rise to a wavy topology of the foliation plane.

For the laboratory seismic measurements we used two different methods:

1) Measurements of P-and S-wave velocities on a sample cube as a function of pressure

Experiments were done in a multi-anvil pressure apparatus at the Institut für Geowissenschaften, Universität Kiel (Germany), allowing simultaneous measurements of compressional (Vp) and orthogonally polarised shear wave velocities (Vs1, Vs2) in the three structural directions *X*, *Y* and *Z* (for details see Kern et al, 1997). Each set of results is composed of nine velocities: three P-wave velocities and six S-wave velocities. Splitting of shear waves is obtained for each direction by two sets of the orthogonally polarized transducers. We used the ultrasonic pulse transmission technique for the velocity measurements with transducers operating at 2 MHz and 1 MHz for P- and S-waves, respectively. The precision of timing measurements is +/− 5 ns, and the timing accuracy is assumed to be better than +/− 0.5%. Length and resulting volume changes of the sample cube, due to changes of principal stress, are obtained by the piston displacement.

2) Measurement of P-wave velocities on a spherical sample as function of pressure

Measurements on the sample sphere were performed at the Institute of Geology in Prague. Spherical samples allow the measurement of P-wave velocities in many sample directions with the same accuracy (Pros et al., 1998). Placing the experimental equipment—consisting of transducers and 3D sample positioning system—in a pressure vessel, the dependence of the P-wave velocities on confining pressure may be determined up to 400 MPa (Pros et al., 2003). The frequency of applied transducers is 2 MHz. In practice, the measurement is conducted on a net dividing the sphere in steps of 15° defining 132 independent measuring directions. The travel-times of ultrasonic signals are measured for all 132 directions at several levels of hydrostatic pressure (commonly 10 or 20, 50, 100, 200 MPa). From these data, P-wave velocities are computed and projected from the surface of the sphere onto the lower hemisphere in equal-area projection. The resulting plots provide knowledge on the spatial distribution of P-wave velocities in the sample.

3) LPO measurements by neutron diffraction and calculation of 3D-velocity distribution of P- and S-waves

Neutron diffraction was applied for the determination of the mineral crystallographic preferred orientations of the sample. Neutron diffraction texture analysis is most suitable for bulk texture[1] investigations of large sample volumes, because of high penetration depth and low absorption of neutrons. Measurements were done with the time-of-flight (TOF) texture diffractometer SKAT at the Frank Laboratory of Neutron Physics at JINR (Dubna, Russia). The advantage of TOF neutron diffraction with high instrumental resolution (Ullemeyer et al., 1998) allow to measure the LPO of low symmetric rock-forming minerals (Ivankina et al., 2005). Typical counting times at SKAT for the measurement of polyphase rock sample is 36 h. The quantitative mineral texture analysis and subsequent calculation of bulk elastic properties (3D-velocity distribution of P- and S-waves) are carried out using BEARTEX program (Wenk et al., 1998). Since neutron diffraction can be done on exactly the same spherical (or cubic) sample, the texture-derived velocities can be directly compared with the measured data.

3. Experimental results

3.1. Directional dependence of P- and S-wave velocities as a function of pressure measured on the sample cube

Fig. 2 presents the three P-wave velocities and six S-wave velocities measured in the structural directions *X*, *Y*, and *Z* as a function of pressure up to 600 MPa (corresponding to about 20 km crustal depth). The velocity–pressure relations display the well-known initial steep velocity increase with increasing confining pressure. The non-linear rise is due to progressive closure of microcracks, typically illustrating the pressure sensitivity of P- and S-waves. Linear behaviour is approached at a smaller and smaller rate above about 150 MPa, marking the intrinsic behaviour of the compacted aggregate. Vp is highest parallel to foliation (*XY*-plane) and lineation [*X*] and lowest normal to foliation (parallel to *Z*). The significant differences of P-wave velocities measured in the three structural directions indicate strong velocity anisotropy (A-Vp), which is defined by the percent differences between maximum and minimum velocity with respect to the mean velocity (Birch, 1961). The change of velocity anisotropy with increasing pressure is evident from Fig. 2a. A-Vp is highest at low pressures. Increasing confining pressure reduces anisotropy in a non-linear slope approaching constant values above about 150 MPa.

Another diagnostic phenomenon for anisotropy is shear wave splitting. A single shear wave propagating through an anisotropic material will be split into approximately orthogonal polarizations,

[1] Here, texture is used as a synonym for crystallographic (lattice) preferred orientation (LPO).

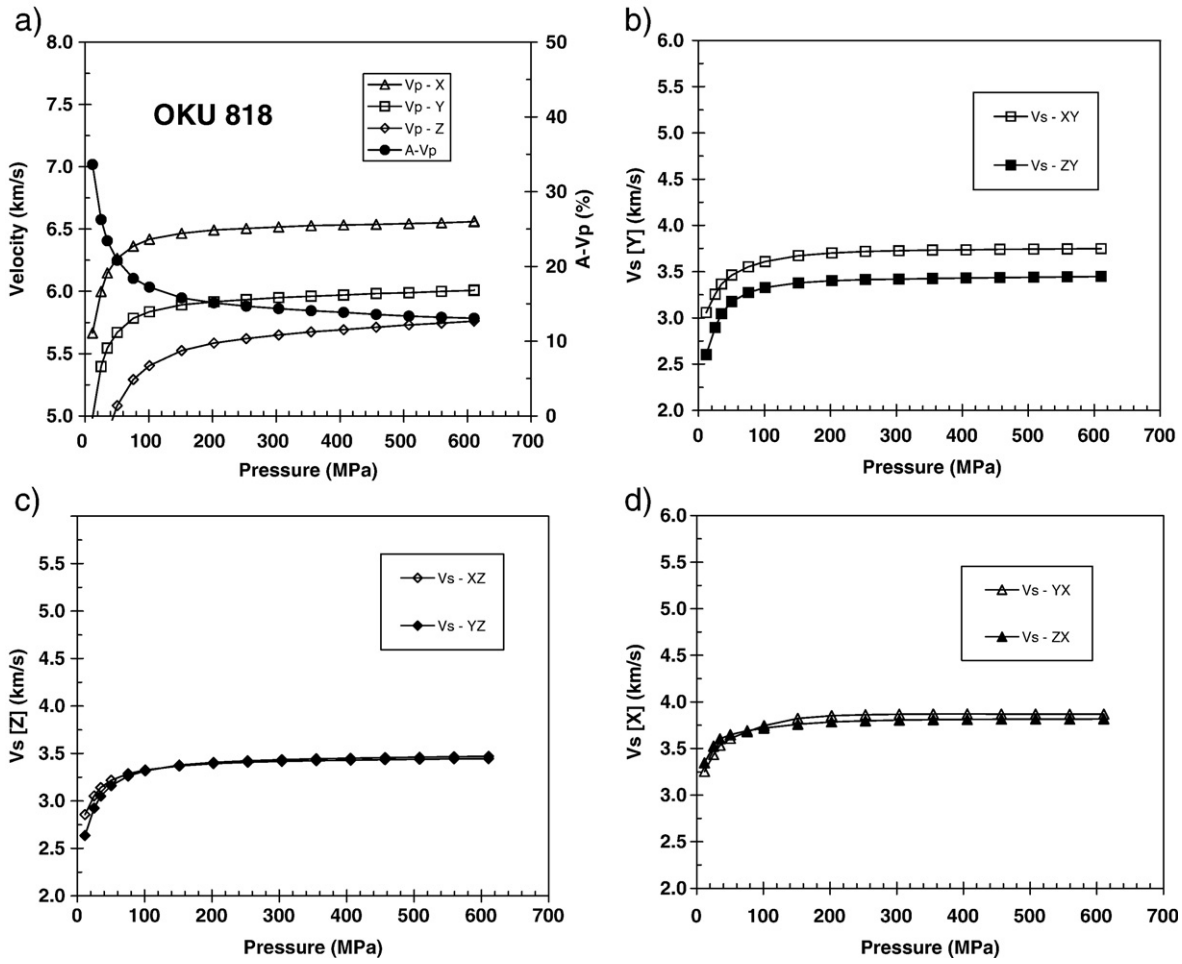

Fig. 2. Pressure dependence of P- and S-wave velocities and P-wave anisotropy (A-Vp), measured in the three structural directions *X*, *Y*, *Z* of the sample cube.

which travel at different velocities (Vs1,Vs2) in the same direction (Crampin, 1987). Fig. 2b–d shows that shear wave splitting is closely related to foliation. It is highest parallel to foliation in the *Y*-direction with the fast split shear wave being polarized parallel to foliation. Normal to foliation (parallel to *Z*) there is practically no shear wave splitting observed. In this direction the samples behaves quasi-isotropic for shear waves.

The 3D velocity distribution obtained from the measurements on the spherical sample is presented in Fig. 3. A strong directional dependence of P-wave velocities is apparent. The velocity surfaces exhibit roughly orthorhombic symmetry with *YZ* and *XY* (foliation plane) as symmetry planes. Velocities are highest parallel to foliation and lowest normal to it. The comparison of the velocity surfaces measured at 0.1, 50. 100 and 200 MPa confining pressure indicates a rapid increase in P-wave velocity and a coeval decrease in P-wave anisotropy with increasing confining pressure. It is important to note that the symmetry of the patterns does not change with pressure. The strong raise of Vp with pressure confirms the marked pressure sensitivity of P-wave velocity observed already by the measurements on the sample cube in the multi-anvil apparatus as well as the close relationship of maximum and minimum velocities to the foliation plane.

3.2. Calculated 3D velocity distributions based on neutron diffraction texture measurements

From the pole figures obtained by the neutron diffraction measurements we derived the orientation distribution functions (ODFs) and recalculated the pole figures for the predominant mineral phases applying the WIMV method (Matthies, 2002). Selected recalculated pole figures of biotite, quartz, plagioclase are shown in

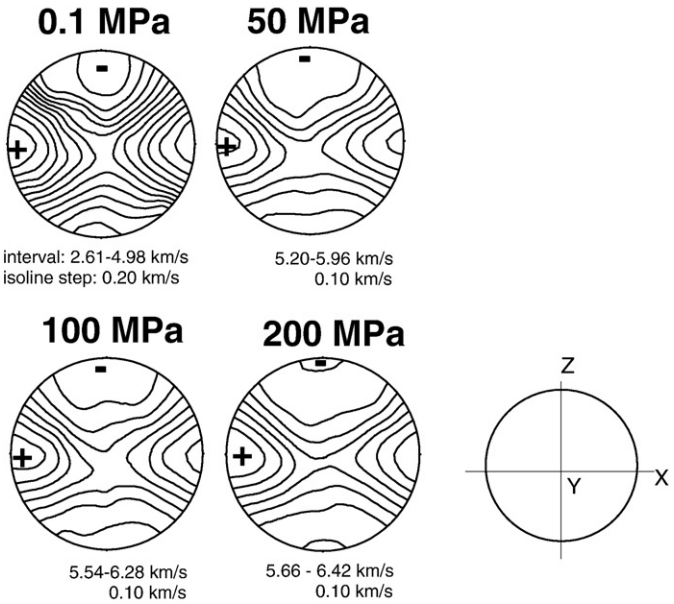

Fig. 3. P-wave distribution in the sample sphere measured at pressures of 0.1, 50, 100, 200 MPa. The foliation-related structural reference frame is indicated.

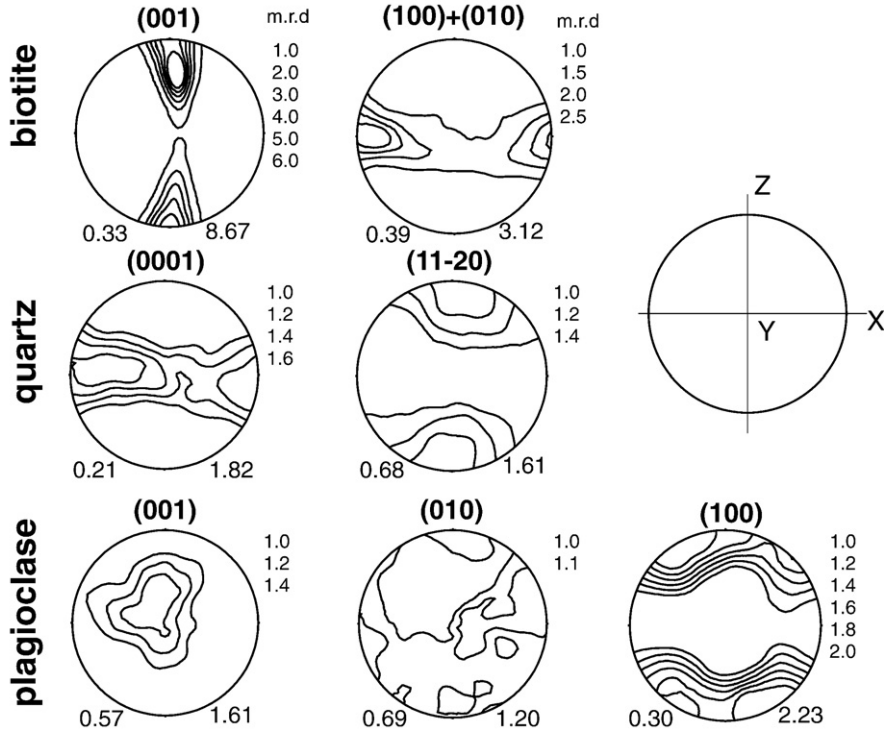

Fig. 4. Recalculated pole figures of the major minerals biotite, quartz, and plagioclase derived from neutron diffraction measurements. Equal area projection, pole density contours in multiples of random distribution (m.r.d).

Fig. 4. Pole densities are normalized so that the integral over a pole figure is 1 and densities are expressed in multiples of a random distribution (m.r.d). The pole figure (001) of biotite shows a strong single maximum normal to foliation with a large angular spread towards *Y*. The poles of the (010)+(100)-planes are concentrated on a great circle subparallel to the foliation plane. The LPOs of quartz and

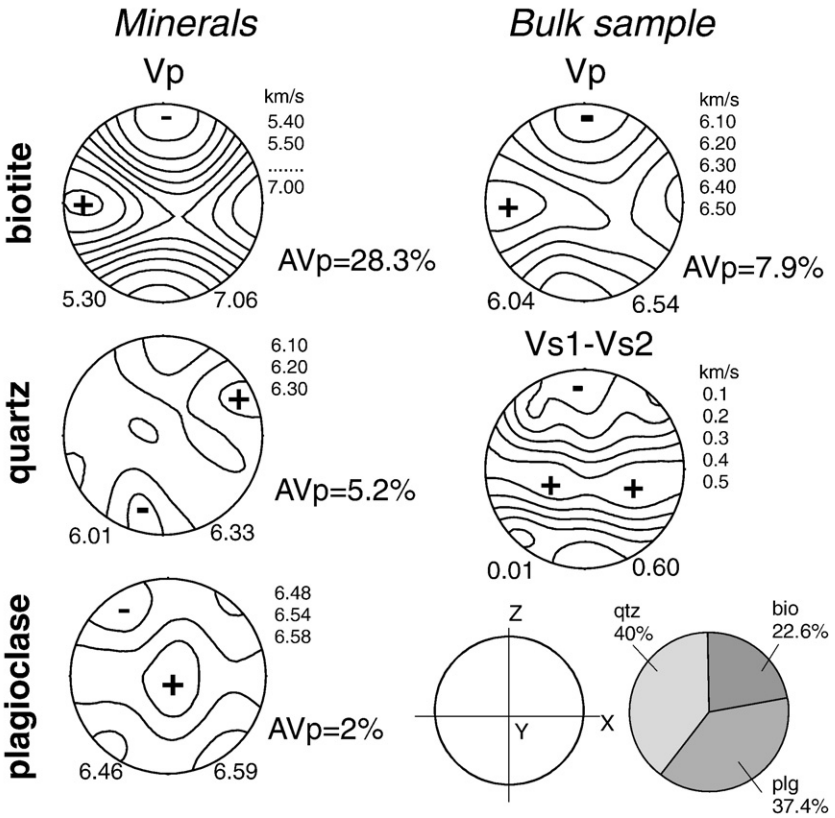

Fig. 5. Calculated velocity surfaces of Vp and Vs1–Vs2 for the mineral aggregates (a) (100 vol.%) and of the whole rock (b).The modal composition of the rock is displayed by the pie diagram.

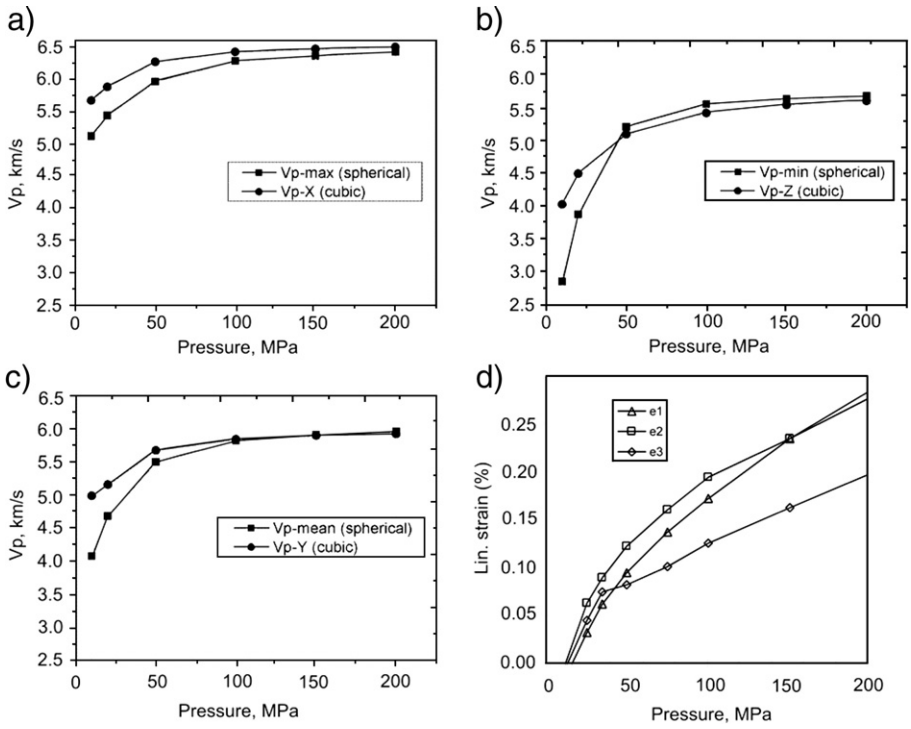

Fig. 6. Comparison of Vp measured on the sample cube in the *X*, *Y*, and *Z* direction with the maximum, mean and minimum velocities measured on the spherical sample for the pressure range of 20–200 MPa along with the linear strain curves derived from the piston displacement in the multi-anvil apparatus.

plagioclase are also well pronounced but much weaker. The normals to the (0001) quartz planes occupy a broad great circle parallel to foliation and the (11–20) normals a broad single maximum perpendicular to it. The pole figures of plagioclase are characterized by a broad single maximum of the (001) poles subparallel to the *Y*-direction and a partial occupation of the (100) poles on of a great circle girdle within the projection plane.

The elastic properties of the polycrystal were obtained by averaging single-crystal properties over the orientation distribution (Bunge, 1985) Based on the Christoffel equation, which combines velocity (*V*), the single-crystal stiffness coefficient (C_{ijkl}) , and the density (rho) we calculated the 3D velocity distributions using the Voigt averaging approach. The Voigt method was applied because it gives the closest agreement between LPO-derived and laboratory-measured seismic velocities (Seront et al., 1989). The single-crystal elastic stiffness coefficients used for the calculation are those reported by Ryzhova (1964) for plagioclase (An29), by Aleksandrov and Ryzhova (1961) for biotite, and by McScimin et al. (1965) for quartz. Fig. 5 presents the LPO-based calculation of Vp velocity surfaces (100 vol.%) for biotite, quartz and plagioclase and the resulting bulk Vp and Vs1–Vs2 (shear wave splitting) for the investigated sample, according to the volume fraction of the constituent minerals. A strong relation of maximum and minimum velocities and shear wave splitting to the foliation plane is displayed by the velocity surfaces, confirming the observations made in the seismic measurements.

4. Discussion

The fine-grained biotite gneiss of a core sample from the Outokumpu Scientific Deep Drill Hole exhibiting strong crystallographic (LPO) and shape preferred orientation (SPO) of the biotite minerals provides an excellent material to investigate the relative contribution of oriented cracks, crystallographic (lattice) preferred orientation (LPO) and shape preferred orientation (SPO) to P- and S-wave velocities, bulk anisotropy and shear wave splitting.

The velocity measurements on a cube-shaped sample in the multi-anvil pressure apparatus (Kiel) as well as on a sample sphere in a pressure vessel (Prague) show a strong pressure sensitivity of both, wave velocities and velocity anisotropy. Fig. 6a–c compares the P-wave velocities measured in the three structural directions *X*, *Y*, and *Z* by the two different techniques for the pressure range of 20–200 MPa. A marked pressure dependence of P-wave velocity (Fig. 6a–c) is seen on both slopes, although the pressure sensitivity of the spherical sample is found to be significantly higher in the very low pressure range. This may be explained, at least in part, by the fact that velocities could not be corrected for the pressure dependent volume change (length change) with this technique. The non-linear steep velocity increase with pressure is clearly a result of progressive closure of microcracks as may also be inferred from the similar slope of the linear strain curves measured by the piston displacement in the multi-anvil apparatus (Fig. 6d).

Fig. 7 compares the pressure sensitivity of Vp-anisotropy for the pressure range of 20–200 MPa obtained by the two different laboratory

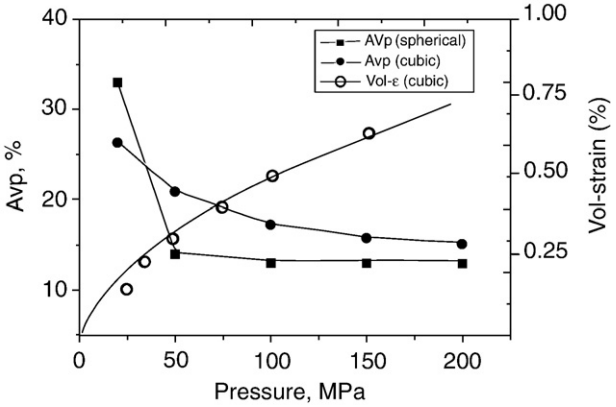

Fig. 7. Comparison of the pressure dependence of P-wave anisotropy obtained by the two methods along with the volumetric strain curve derived from the piston displacement in the multi-anvil apparatus.

Table 1
Comparison of measured (at 200 MPa) and calculated P-velocities (km/s), shear wave splitting Vs1–Vs2 (km/s) and P-wave anisotropy AVp (%) for the three directions *X*, *Y*, *Z*

Method	*X*		*Y*		*Z*		AVp
	Vp	Vs1–Vs2	Vp	Vs1–Vs2	Vp	Vs1–Vs2	
Measurement on a *spherical* sample	6.43	–	5.92	–	5.66	–	13.0
Measurement on a *cubic* sample	6.49	0.07	5.95	0.30	5.57	0.01	15.1
Calculations based on neutron diffraction	6.53	0.52	6.42	0.46	6.05	0.05	7.9

techniques. On both curves P-wave anisotropy is highest at low pressure and decreases in a non-linear slope approaching constant values above about 150 MPa. In the low pressure range, oriented low-aspect ratio microcracks are an important contribution to bulk anisotropy. The pressure dependent non-linear decrease of P-wave anisotropy results from the progressive closure of oriented microcracks. This is clearly indicated by the inverse slope of the volumetric strain curve derived from the piston displacement (Fig. 7). A major contribution is from the biotite microstructure, where intercrystalline and intracrystalline cracks are closely related with the biotite minerals, occurring mainly parallel to the morphologic sheet plane (001). Therefore, effects from oriented microcracks and single-crystal properties both are additive and enhance anisotropy at low pressure. The close linkage between oriented cracks and the biotite crystallographic fabric is also evident from the experimentally determined velocity surfaces presented in Fig. 3. Increasing pressure and coeval crack closure increases Vp and decreases A-Vp, but does not change the orthorhombic symmetry of the Vp velocity distribution, due to a symmetrical superimposition of both fabrics. Above about 150 MPa the effect of oriented cracks is almost eliminated and the residual (intrinsic) anisotropy is mainly due to crystallographic (LPO) and probably to shape preferred orientation (SPO).

The influence of preferred orientation of the rock-forming minerals to anisotropy is twofold. First, there is a direct influence of intrinsic single-crystal elastic properties which is unaffected by pressure except for the small change of single-crystal elastic properties with pressure. The second contribution is from their lattice preferred orientation (LPO). The LPO-based model velocity distribution presented in Fig. 5 allows us to discriminate the relative contribution of the rock-forming minerals to the bulk intrinsic anisotropy of the rock. The velocity surfaces calculated for the partial fabrics (aggregates; 100 vol.%) of biotite, quartz, and plagioclase (Fig. 5 left) display most distinctly which minerals mainly contribute to bulk anisotropy. It is clear from Fig. 5 (left) that the LPO-related velocity anisotropy is dominated by the biotite texture. The biotite component, which constitutes about 23 vol.% has the strongest preferred orientation and also the strongest anisotropy of single-crystal velocities (44%) versus quartz (27%) and plagioclase (29%). Note that quartz and plagioclase and their orientation fabrics superimpose more or less in a constructive way, but their contribution to bulk anisotropy is of second order.

The LPO-based velocity calculations also confirm the close relationship between intrinsic seismic anisotropy, shear wave splitting and inherent structural elements (foliation, lineation) derived from the experiments in the multi-anvil apparatus (Fig. 2 b–d) as well as in the pressure vessel (Fig. 3). It is apparent from the shear wave splitting stereogram presented in Fig. 5 (right) that (Vs1–Vs2) is highest in the *Y*-direction subparallel to foliation and lowest normal to it. The markedly smaller shear wave splitting measured parallel to the *X* direction can by explained by the large angular spread of the biotite (001) normals) towards *Y* (Fig. 4) confirming the fluctuation in the orientation of the platy biotite crystals around *X* documented in Fig. 1b. Therefore, the particle motion of the two shear waves S1 and S2 propagating in the *X* direction is more or less oblique to the (001) normals of many biotite minerals. As a consequence, the difference in shear wave velocities recorded by the two receiving transducers is only small (for further information see Ivankina et al., 2005).

Table 1 summarizes important measured and calculated data for the three structural directions *X*, *Y*, and *Z* for comparison. It is evident that measured P-wave velocities are lower and anisotropies are higher than those inferred from LPO patterns derived from the neutron diffraction texture measurements. By contrast, shear wave splitting is higher in the model calculation. The marked differences between calculated and measured velocities and velocity anisotropy are also documented in Fig. 8 where we compare the 3D model velocity distribution with the velocity surface derived from the measurements (200 MPa) on the spherical sample. Although the shape of both stereo-plots are very similar, they exhibit large differences in Vp and P-wave anisotropy values. The likely reason for this is that in our polyphase averaging neither effects of grain shape and intergrain spherical (high aspect ratio) pores are taken into account that would lower elastic stiffness and correspondingly acoustic velocities (e.g. Ponte Castabneda and Willis, 1995; Sayers, 1994). Furthermore, minor phases were not considered in the calculation. Nevertheless, the high intrinsic P-wave anisotropy of about 15% measured above the crack-closing pressure (>150 MPa) which is nearly the double of the calculated one (about 8%) can only in part be explained by the contribution of preferred mineral orientation. Obviously, the measured intrinsic seismic properties of the foliated rock cannot be modeled simply as volume averages of the aggregate based on orientation and volume fractions of the constituent minerals. It should also be noted that part of the differences between calculated and measured anisotropy could be due to the calculating procedure and the poorly known properties of biotite and plagioclase. Nevertheless, we suggest that shape preferred orientation (SPO) of the oriented crystals, in particular of biotite, contributes substantially to bulk velocity anisotropy, in addition to the LPO. Burlini and Kunze (2000), in their study on Carrara marble mylonite, could also show that shape preferred orientation of elongated calcite minerals contributed largely to the measured bulk anisotropy.

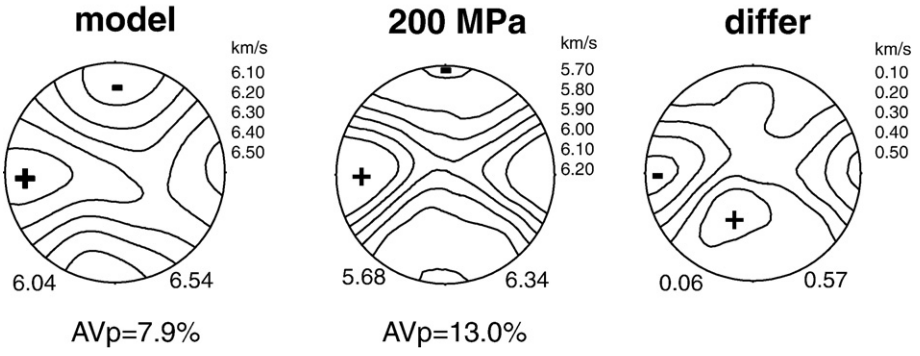

Fig. 8. Comparison of calculated (model) and measured (200 MPa) 3D distribution of P-wave velocities and velocity anisotropy.

5. Conclusions

The strongly foliated biotite gneiss sample from the Outokumpu scientific drill hole provides an excellent material to document the influence of microstructural and textural properties on rock anisotropy. Laboratory seismic measurements on a sample cube in a multi-anvil pressure apparatus as well as on a sample sphere in a pressure vessel confirm a marked pressure sensitivity of P- an S-wave velocities. At low effective pressure, oriented microcracks contribute largely to the directional dependence of elastic wave velocities, in addition to crystallographic (LPO) and shape preferred orientation (SPO) of minerals. Most important is biotite which displays the strongest preferred orientation, compared to the constituent quartz and plagioclase minerals and also the strongest anisotropy of single-crystal velocity. Importantly, inter- and intracrystalline cracks of biotite are closely linked to the (001) morphologic sheet plane. Consequently, oriented microcracks superimpose the crystallographic and shape fabric in a constructive way and thus give rise to very high anisotropy at low pressure. At conditions of high pressure (>150 MPa) where most of the low-aspect ratio cracks are closed, the residual velocity anisotropy is mainly caused by crystallographic (LPO) and shape preferred orientation (SPO). From the velocity calculations based on neutron diffraction texture measurements it is clear that the LPO-related intrinsic velocity anisotropy is dominated by the biotite LPO. The contribution of the constituent quartz and plagioclase minerals is very weak. The LPO-based model calculation suggests that the experimentally determined Vp-anisotropy for the compacted aggregate cannot be explained by the crystallographic preferred orientation of major minerals (LPO) alone. We suggest that a major contribution is from the strong SPO of biotite and further grain boundary effects.

Acknowledgements

We thank D. Schulte-Kortnack (Kiel) for help with the experiments in the multi-anvil apparatus. I. Kukkonen (Geological Survey of Finland) provided sample material, K. Mengel (Clausthal) the chemical analysis and the thin sections, and A. Fehler prepared the sample cube. Reviews by M. Savage and an anonymous reviewer are greatly appreciated. Part of this research was supported by the Russian Foundation for Basic Research (Grant No 07-05-oo303), by AS CR project No.: Z 3013 0516 and by Czech Science Foundation (Grant. No.: 205/08/0676.

References

Aleksandrov, K.S., Ryzhova, T.V., 1961. The elastic properties of rock forming minerals. II. Layered silicates. Izv. Acad. Sci. USSRGeophys. Ser. 12, 1799–1804 (in Russian).

Barruol, G., Kern, H., 1996. Seismic anisotropy and shear wave splitting in lower-crustal and upper mantle rocks from the Ivrea zone — experimental and calculated data. In: Mainprice, D., Vauchez, A. (Eds.), Dynamics of the Subcontinental Mantle: From Seismic Anisotropy to Mountain Building. Phys. Earth and Planet. Inter., 95, pp. 175–194.

Burlini, L., Fountain, D.M., 1993. Seismic anisotropy of metapelites from the Ivrea–Verbano zone and Serie dei Laghi (N. Italy). Phys. Earth Planet. Inter. 78, 301–317.

Burlini, L., Kunze, K., 2000. Fabric and seismic anisotropy of Carrara marble mylonite. Phys. Chem. Earth (A) 25, 133–139.

Birch, F., 1961. The velocity of compressional wave velocities in rocks to 10 kbar, part 2. J. Geophys. Res. 66, 2199–2224.

Bunge, H.-J., 1985. Physical properties of polycrystals: chapter 24. In: Wenk, H.R. (Ed.), Preferred Orientation in Deformed Metals and Rocks: An Introduction to Modern Texture Analysis. Academic Press, Orlando, pp. 507–525.

Christensen, N.I., 1984. The magnitude, symmetry and origin of upper mantle anisotropy based on fabric analyses of ultramafic tectonites. Geophysical Journal of the Royal Astronomical society 76, 89–111.

Crampin, S., 1987. The geological and industrial implications of extensive-dilatancy anisotropy. Nature 328, 491–496.

Ivankina, T.I., Kern, H., Nikitin, A.N., 2005. Directional dependence of P- and S-wave propagation and polarization in foliated rocks from the Kola superdeep well: evidence from laboratory measurements and calculations based on TOF neutron diffraction. Tectonophysics 407, 25–42.

Kern, H., Liu, B., Popp, T., 1997. Relationship between anisotropy of P- and S-wave velocity and anisotropy of attenuation in serpentinite and amphibolite. J. Geophys. Res. 102, 3051–3065.

Kern, H., Popp, T., Gorbatsevich, F., Zharikov, A., Lobanov, K.V., Smirnov, Yu, P., 2001. Pressure and temperature dependence of Vp and Vs in rocks from the superdeep well and from surface analogues at Kola and the nature of velocity anisotropy. Tectonophysics 338, 113–134.

McScimin, H.J., Andreatch, P., Thurston, N.R., 1965. Elastic moduli of quartz versus hydrostatic pressure at 5 and – 195.8 °C. J. Appl. Phys. 36, 1624–1632.

Matthies, S., 2002. 20 years WIMV, history, experience and contemporary developments. Mat. Sci. Forum 408–412, 95–100.

Ponte Castabneda, P., Willis, J.R., 1995. The effect of spatial distribution on the effective behavior of composite materials and cracked media. Journal of Mechanics and Physics of Solids 43, 1919–1951.

Pros, Z., Lokajicek, T., Klima, K., 1998. Laboratory study of elastic anisotropy on rock samples. Pure and Applied Geophysics 151, 619–629.

Pros, Z., Lokajicek, T., Prikryl, R., Klima, K., 2003. Direct measurement of 3D elastic anisotropy on rocks from the Ivrea Zone (Southern Alps, NW Italy). Tectonophysics 370, 31–47.

Ryzhova, T.V., 1964. Elastic properties of plagioclase. Bull. Acad. Sci. USSR Geophys. 633–635 Ser. 7.

Sayers, C.M., 1994. The elastic anisotropy of shales. J. Geophys. Res. 99, 767–774.

Seront, B., Mainprice, D., Christensen, N.I., 1989. The complete seismic properties of anorthosite: comparison between LPO and laboratory measurements. EOS 70, 460–461.

Ullemeyer, K., Spalthoff, P., Heinitz, J., Isakov, N.N., Nikitin, A.N., Weber, K., 1998. The SKAT texture diffractometer at the pulsed reactor IBR-2 at Dubna: experimental layout and first measurements. Nucl. Instrum. Methods. Phys. Res. A 412/1, 80–88.

Wenk, H.-R., Matthies, S., Donovan, J., Chateigner, D., 1998. BEARTEX: a windows-based program system for quantitative texture analysis. J. Appl. Crystallogr. 31 362–269.